# Catalysis Science & Technology

Accepted Manuscript






ROYAL SOCIETY OF CHEMISTRY

www.rsc.org/catalysis

# Catalytic Hydrodeoxygenation of Palmitic Acid over Bifunctional Co-doped $MoO_2$/CNTs Catalyst: an Insight into the Promoting Effect of Cobalt

Ranran Ding[a], Yulong Wu[a,b]*, Yu Chen[a], Hao Chen[c], Jianlong Wang[a], Yanchun Shi[a], Mingde Yang[a]

[a]Institute of Nuclear and New Energy Technology, Tsinghua University, Beijing 100084, PR China
[b]Beijing Engineering Research Center for Biofuels, Beijing 100084, PR China
[c]School of Chemical Engineering and Technology, Xi'an Jiaotong University, Xi'an 710049, PR China

## Abstract

Novel Co-doped $MoO_2$/CNTs catalysts were prepared by wet-impregnation method and employed in catalytic hydrodeoxygenation (HDO) of palmitic acid. The obtained catalysts were systematically characterized using various techniques, namely, XRD, BET surface area, XPS, FT-IR of adsorbed pyridine, Raman, $H_2$-TPD, and $H_2$-TPR. Characterization studies revealed that Co ions doped into the lattice of $MoO_2$, the interaction between metal species modified the electrical properties of the catalytic active sites, and formation of new active sites and defects. Catalytic results showed that, Co ions could significantly improve catalytic performance, and the best selectivity to hexadecane reached 89.3% at an extremely low temperature of 180°C. The increased presence of $Mo_2C$ particles, Lewis acidic sites and oxygen vacancies were all responsible for the noticeable catalytic performance of the Co doped catalyst. The mechanistic insights from this work confirmed the bifunctional role of Co-doped $MoO_2$/CNTs catalysts for HDO of palmitic acid, which was catalyzed either solely by $Mo_2C$ or synergistically by $Mo_2C$ and $MoO_2$. Insights into the nature of the active site would provide a useful knowledge for rational design of effective Mo-based HDO catalysts and assist future studies on more efficient catalytic conversion systems.

**Keywords:** palmitic acids; hydrodeoxygenation; Co-doped； bifunctional

## Introduction

Due to the depletion of fossil resources and rapidly increasing emissions of greenhouse gases, alternative energy sources were developed to produce liquid hydrocarbon fuels.[1,2] The utilization of algal biomass as a source of renewable carbon for the production of hydrocarbon fuels and chemicals had garnered much attention due to its impressive productivity, noncompetition with agriculture, and high carbon

dioxide uptake.[3,4] However, the bio-oil obtained from thermochemical conversion processes of algal biomass cannot be directly used as a liquid transportation fuel because of oil acidity, low heating value, high viscosity, and secondary pollution, all of which are due to its high content of oxygen.[5-7] Therefore, deoxygenation of algal bio-oil had been proved to be an effective method to produce transportation fuels, among which HDO was one of the most potentially valuable processing routes to selectively cleave C-O or C-C bonds in oxygen-containing compounds. [8]

So far, several types of HDO catalysts have been developed. For example, noble metal-based catalysts (e.g. Pd, Pt, Rh, and Ru) supported on activated carbon are active and selective for HDO.[9,10] However, the exorbitant price of the noble metal-based catalysts may hinder their large-scale application, additionally, the adsorption of low-boiling-point compounds on the active sites of the noble metal-based catalyst leads to their deactivation.[11] Therefore, the development of the non-noble metal catalysts for HDO reaction attracts researchers' focus. Recently, Lercher et al. demonstrated that the HDO of microalgae oil to alkanes via cascade reactions over bifunctional catalysts of Ni supported on acidic zeolite.[12] However, the major drawback of Ni-based catalysts was the high activity of C-C bonds rather than C-O bonds, which would decrease the C atom economy. In addition, Ni-based catalysts are active at a relative higher temperature (>260$^{o}$C), which may cause undesired side reactions such as aromatization and coking (some of which can lead to catalyst deactivation).[13] $MoO_x$ have been recently reported to be attractive and effective catalysts for the selective scission of the C-O and C=O bonds in various biomass-derived oxygenates, including aliphatic and cyclic ketones, esters, furanics, and phenolic compounds due to its favorable structural properties, such as mixed oxidation state, adequate lattice defects, high stability, and low cost.[14-16] It has been reported for first time by our group that $MoO_2$/CNTs had higher selectivity and stability in catalytic HDO of long-chain fatty acids.[17] However, high reaction temperatures (230$^{o}$C) are still needed for the totally HDO of the fatty acids into alkanes and the nature of the active site(s) is not identified.

Generally, the introduction of a suitable dopant (or called metal modification) would bring a pronounced enhancement in activity, selectivity, and stability due to the formation of defects, new active sites, acidic or basic sites.[18-22] For instance, Co is selected as a dopant in the Ni-Mo-Co to change the electronic properties of adjacent Mo atoms, resulting in an increase of catalytic activity and satisfactory stability in the

HDO of phenol.[23] Accordingly, in our present work, Co is intentionally selected as the dopant to achieve the metal modification of $MoO_2$/CNTs catalyst to further improve the catalytic performance. First, Co-doped $MoO_2$/CNTs and pristine $MoO_2$/CNTs catalysts were prepared by means of a wet-impregnation method. Second, systematic characterizations were conducted to explore the effect of Co as a dopant on the structure and properties of $MoO_2$/CNTs and to reveal the nature and genesis of surface active sites. Finally, the reusability of Co-doped $MoO_2$/CNTs catalyst was investigated for the HDO of palmitic acid to study its stability and deactivation mechanism. Understanding the role of dopant was extremely helpful in tailoring the active centers and might be extended to guide the design of more efficient heterogeneous catalysts for the direct HDO of algal-based bio-oil to transportation fuels.

## Experimental section

### Materials

CNTs were generously provided by Xianfeng Advanced Material Supplier (Nanjing, China). Decane (>99%) and palmitic acid (99.0%) were purchased from Guangfu Fine Chemical Research Institute (Tianjin, China). Ammonium molybdate (99.0%) was purchased from Guang fu Technology Development Co., Ltd. (Tianjin, China). Co $(NO_3)_2 \cdot 2H_2O$ was purchased from Civi-Chem Technology Co., Ltd. (Shanghai, China). All reagents were used as-received without further purification.

### Catalyst preparation

The pristine 5% wt.$MoO_2$/CNTs and 1.5% wt. Co-doped $MoO_2$/CNT catalysts were synthesized by an incipient wetness impregnation method. In a representative procedure, the desired quantities of $(NH_4)_6Mo_7O_{24} \cdot 4H_2O$ and Co $(NO_3)_2 \cdot 2H_2O$ were dissolved in distilled water and then slowly dropping this solution onto CNTs with continuous stirring. After allowing the metal to incorporate into the support over 4 h at ambient temperature, the excess water was evaporated on a hot plate under vigorous stirring. The obtained products were oven dried at 105 °C for 12 h and calcined at 500 °C for 3 h (ramp: 10 mL $min^{-1}$) in air atmosphere. Thereafter, they were reduced at 500 °C for 4 h (ramp: 10 °C $min^{-1}$) in hydrogen (flow rate: 80 mL

$min^{-1}$). The required reduction temperatures were determined by $H_2$-TPR. For convenience, the prepared samples were denoted as Mo-X or CoMo-X throughout the article, in which X refers to the reduction temperature.

**Catalyst characterization**

XRD patterns were measured on a D8 ADVANCE diffractometer using Cu Kα radiation ($\lambda$= 0.1541 nm, 36 kV, 2 mA, scanning step = 2° $min^{-1}$). The diffraction patterns were recorded by scanning at an angle ranging from 0° to 80°. Specific surface area analysis of the catalyst was performed by nitrogen sorption isotherms at -196 °C in a Micromeritics Tristar analyzer. Pretreatment of samples for surface area measurement was done by flowing $N_2$ for 6 h at 300 °C. The surface areas were calculated by the Brunauer-Emmett-Teller (BET) method, and the pore size distribution was calculated by the Barrett-Joyner-Halenda (BJH) method.

Raman spectra were recorded at room temperature on a Horiba Jobin-Yvon HR800 Raman spectrometer equipped with a liquid-nitrogen cooled charge coupled device (CCD) detector and a confocal microscope. The line at 514 nm of $Ar^+$ ion (Spectra Physics) laser was used as an excitation source for the visible Raman spectroscopy. The laser was focused on the sample under a microscope with the diameter of the analyzed spot being ~1μm. The acquisition time was adjusted according to the intensity of Raman scattering. The wavenumber values reported from the spectra were accurate to within 1 $cm^{-1}$. The FT-IR absorption spectra were obtained with a Bruker model Tensor 27 equipment in the range of 4000-400$cm^{-1}$, using KBr powders. Fourier transform infrared spectroscopy of adsorbed pyridine on the catalysts were recorded on a NEXUS 670 FTIR spectrometer. Before measurement, the catalyst sheets were evacuated at 200 $^oC$ for 2 h under vacuum of $10^{-2}$ Pa and then cooled to ambient temperature. After pyridine adsorption for 30 min and evacuation at 100 $^oC$ for 1 h, IR spectra were recorded.

TPR was conducted with a TP-5076 multiple adsorption instrument (Xian-quan, China). It was performed at a rate of 5 $^oC \cdot min^{-1}$ from room temperature to 800 $^oC$ in a flow of 5% $H_2/N_2$. The consumption of $H_2$ was analyzed online with a thermal

conductivity detector (TCD).Temperature-programmed desorption of hydrogen ($H_2$-TPD) experiment was carried out in a TP-5076 multiple instrument. The sample (0.10 g) was packed into a reactor with quartz tubing, and was treated at 500 $^oC$ in a flow of He (30 $mL \cdot min^{-1}$) for 1 h and adsorbed a flow of $H_2$ (15 $mL \cdot min^{-1}$) at 50$^oC$ for 30 min, and then purged with He until the physically adsorpted $H_2$ was removed. The sample was then heated under a flow of He (30$mL \cdot min^{-1}$) from 50 $^oC$ to 800 $^oC$ with a ramp of 10 $^oC \cdot min^{-1}$. The signals of $H_2$-TPD were recorded with an online thermal conducted detector (TCD).

XPS was performed on an AMICUS spectrometer (KRATOS, England). The X-ray source utilized was Mg Kα (1253.6 eV) radiation. Analysis was done at room temperature, and the samples were maintained under rigorous vacuum typically in the order of less than $10^{-8}$ Pa to avoid large amount of noise in the spectra from contaminates. All binding energies measured were within a precision of ±0.2 eV. The binding energies were corrected by setting the binding energy (BE) of the adventitious carbon (C 1s) peak at 284.6 eV.

The final liquid phase products were analyzed in an Agilent GC-MS (6820) with a GsBP-Inowax (30 m × 0.32 mm × 0.25 μm) column and a flame ionization detector. One microliter of the sample was injected into the GC at a split ratio of 10:1, and the carrier gas (helium) flow rate was 10 mL $min^{-1}$. The oven temperature program started at 120 °C for 2 min, and then ramped to 260 °C at a rate of 10 °C $min^{-1}$ held for 10 min at this temperature. Quantitative analysis of liquid products was conducted using the external standard method. The vapor phase was analyzed online by a gas chromatograph with TCD detector and capillary column (Porapak Q).

**Catalytic tests**

Catalytic experiments with palmitic acid were carried out in a 150 mL autoclave in batch mode. A typical reaction was conducted as follows: reactant (0.5 g), decane (50 mL), and catalyst (0.1 g) were loaded onto the autoclave, which was then purged with the gas at ambient temperature and the pressure was adjusted to 4 Mpa prior to the reaction. Finally, the mixture was heated to 200 °C under stirring at 300 rpm to

start the reaction.

Conversion = (moles of converted palmitic acid/mole of the starting palmitic acid) × 100%. Component distribution = (moles of each component/mole of total component) ×100%.

**Catalyst recycling**

When the reaction was complete, the catalyst was deposited at the bottom of the autoclave. The precipitate was separated by filtration and then dried under air atmosphere in an oven at 105 °C for 10 min. The catalyst was recovered and reused in the next run without further activation treatment. We also dried the catalyst under vacuum atmosphere, and find the dried atmosphere almost no effect on catalyst performance.

**Results and discussion**

**Synthesis of Co doped $Mo_2O$/CNTs**

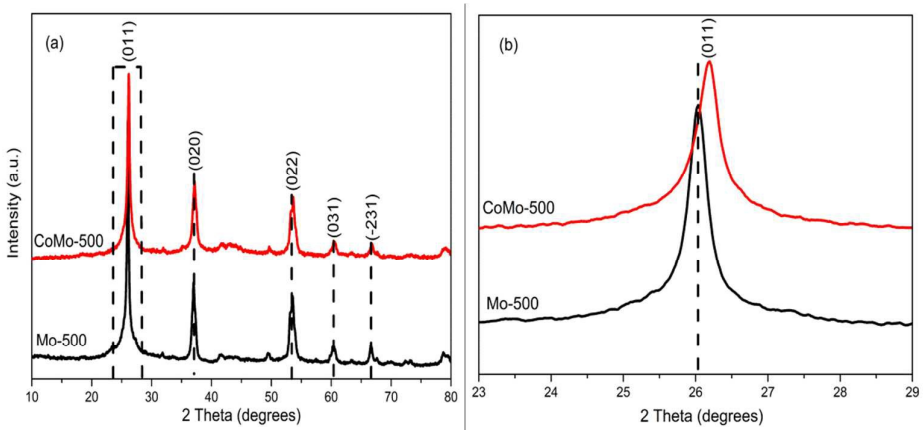


Fig. 1. (a) Powder X-ray diffraction patterns of Mo-500 and CoMo-500 samples and (b) the enlarged X-ray diffraction patterns of the selected areas.

The XRD patterns of Mo-500 and CoMo-500 catalysts were shown in Fig. 1(a). Both Mo-500 and CoMo-500 had similar diffraction peaks at $2\theta$ = 26°, 37°, 53°, 60°, and 67°, which were assigned to the planes of (011), (020), (022), (031), and (-231) of monoclinic $MoO_2$ phase, respectively (JCPDS: 65-1273). No diffraction peaks corresponding to Co or Co-oxides were observed in the investigated XRD region. The notable scrutiny can be explained due to either doping of Co ions into the $MoO_2$

lattice or the amorphous nature of the impregnated Co- and Co-oxides. Fig. 1(b) reveals that the XRD peaks of the CoMo-500 sample were broader and shifted to higher angles compared to those of pristine $MoO_2$. The lattice parameters of the two catalysts were calculated in Table 1, obviously, the lattice parameters decreased. The peaks shifted towards higher angles and lattice contraction (i.e., smaller lattice parameters), which might be elucidated by the doping of smaller sized $Co^{3+}$ ions into the $MoO_2$ lattice. These disparate features, such as peak shift, variation in the lattice parameters, and absence of peaks assigned to Co-oxides obviously confirmed the formation of Co-doped $MoO_2$ solid solutions. The formation of the possible defects in this system is depicted in Scheme 1.

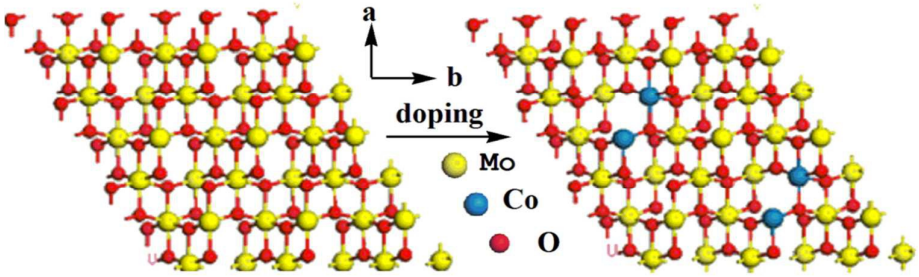


Scheme 1. Defects patterns in Co-doped $MoO_2$ lattice.

In addition to defects caused by Co doping, lattice distortion is also expected in the CoMo-500 sample. The values of lattice distortion were calculated by the formula[24]: $(2\beta)^2 \cos^2\theta = 4/\pi^2(\lambda/D_{h\,k\,l})^2 + 32 \langle\varepsilon_{h\,k\,l}^2\rangle \sin^2\theta$, where $D_{h\,k\,l}$ was the average thickness of the lattice face, $\lambda$ was the wavelength of the X-ray used (0.15406 nm), $\theta$ was the diffraction angle of the (h k l), and $\beta$ was the corrected full-width at half-maximum of the diffraction peak, $\langle\varepsilon_{h\,k\,l}^2\rangle^{1/2}$ was the lattice distortion. The lattice distortions values of Mo-500 and CoMo-500 catalysts were estimated as $1.63 \times 10^{-2}$ and $1.89 \times 10^{-2}$, respectively. It was found that CoMo-500 exhibited higher lattice distortion values than that of Mo-500 because of Co ions incorporation into the $MoO_2$ lattice. The average crystallite sizes of $MoO_2$ were determined via the Debye-Scherrer formula [25] (Table 1). Interestingly, it was noted that the crystallite size of $MoO_2$ obviously decreased after doping of Co ions into the $MoO_2$ lattice, which acted as a dopant to inhibit crystal growth.

**Table 1** Average crystallite size, crystal system, lattice parameters, lattice distortion and BET surface area of catalysts

| Catalysts | Crystal system | Lattice parameters | | | | D(nm) | BET($m^2$/g) | $<\varepsilon_{hkl}^2>^{1/2}\times10^2$ |
|---|---|---|---|---|---|---|---|---|
| | | a(Å) | c(Å) | α | β | | | |
| Mo-500 | Monoclinic | 5.84 | 5.91 | 90° | 120° | 13.5 | 130.0 | 1.63 |
| Co-Mo-500 | Monoclinic | 5.82 | 5.86 | 90° | 120° | 10.7 | 128.0 | 1.89 |

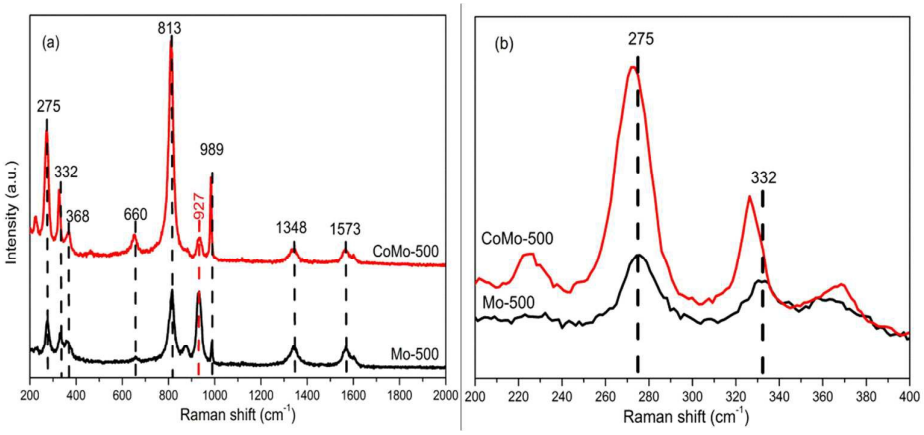


Fig. 2. (a) Visible Raman spectra of Mo-500 and CoMo-500 samples and (b) the enlarged Raman spectrum of samples at low Raman shift.

Raman spectroscopy was considered as a powerful experimental technique for determining the vibrational frequencies and structural properties of the $MoO_2$-based materials.[26] As depicted in Fig. 2(a), six Raman peaks at 275, 332, 368, 660, 813 and 989 $cm^{-1}$ could be assigned to the monoclinic structure of the $MoO_2$. At the same time, the position and relative intensity of the Raman peaks were in good agreement with those reported by Liu.[27] The peaks at around 1348 and 1573 $cm^{-1}$ were assigned to D-band and G-band of CNTs, indicating that the synthesized samples were composites of $MoO_2$ with CNTs.[28] As was shown in Fig. 2(b), some prominent peaks of CoMo-500 sample were shifted to lower wavenumbers than that of Mo-500. According to the literature, [29] doping of smaller metal ions and the consequent lattice contraction of molybdenum oxide as well as M-O vibration frequency might induce such a shift towards lower filed in the peak position. The peak observed at 927 $cm^{-1}$ was ascribed to the O-Mo-O vibrations of the $MoO_4$ tetrahedra of $Mo_4O_{11}$, indicating that the calcined catalyst precursors $MoO_3$ only partially reduced.[30] It was obvious from the Fig. 2(a) that the amount of $Mo_4O_{11}$ in Mo-500 was more than that of CoMo-500 catalyst, suggesting that the Co-dopant facilitate the reduction of Mo

species.

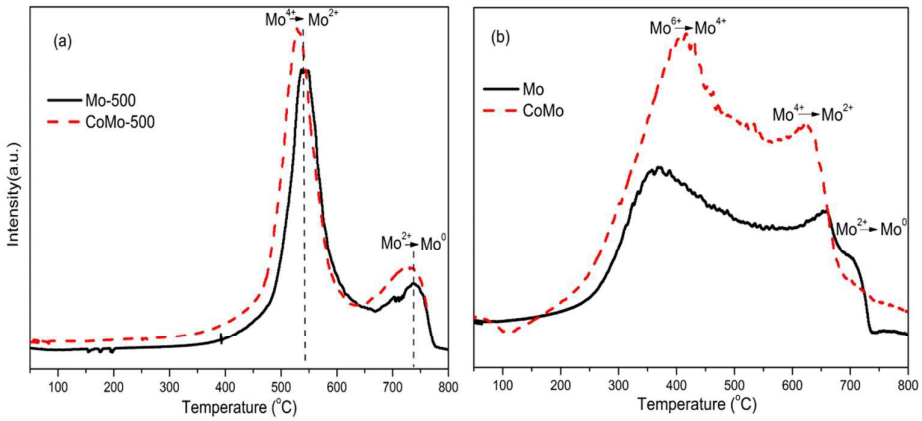


Fig.3. (a) $H_2$-TPR patterns of Mo-500 and CoMo-500 samples and (b) the $H_2$-TPR patterns of calcined precursors.

Hydrogen temperature-programmed reduction ($H_2$-TPR) was performed to study the effect of Co addition on the reducibility of the $MoO_2$ and the reactivity of oxygen in $MoO_2$ lattice. As was shown in Fig. 3(a), both Mo-500 and CoMo-500 catalysts exhibited two prominent peaks at ~530 and ~726°C, which were assigned to the stepwise reduction of $Mo^{4+}\rightarrow Mo^{2+}$ and $Mo^{2+}\rightarrow Mo^{0}$, respectively. Interestingly, the substitution of $Mo^{4+}$ by Co ions led to shift of reduction peaks towards lower temperature, and the total quantity of desorbed oxygen from the CoMo-500 catalysts was more than that of Mo-500. The improved reducibility of Co-doped catalysts was due to structural modifications induced in the $MoO_2$ lattice when some Co ions were incorporated in the $MoO_2$ lattice and generated lattice defects (such as oxygen deficiency), thus favoring the diffusion of $O^{2-}$ anions within the lattice and facilitate the $MoO_2$ reduction. Moreover, some defects such as oxygen deficiency and dislocation on the surface of $MoO_2$ crystals with relatively low activation energy could facilitate the $MoO_2$ reduction.[31] The reduction properties of calcined catalyst precursors were also studied by $H_2$-TPR technique (Fig. 3(b)). Considering the results of Raman and $H_2$-TPR, the reduction steps of catalyst precursors ($MoO_3$) were summarized by following reactions:

$$4MoO_3 + H_2 \rightarrow Mo_4O_{11} + H_2O \quad (1) \qquad Mo_4O_{11} + H_2 \rightarrow 4MoO_2 + H_2O \quad (2)$$

$$MoO_2 + 2H_2 \rightarrow Mo^{2+} + 2H_2O \quad (3) \qquad Mo^{2+} + H_2 \rightarrow Mo^{0} + H_2O \quad (4)$$

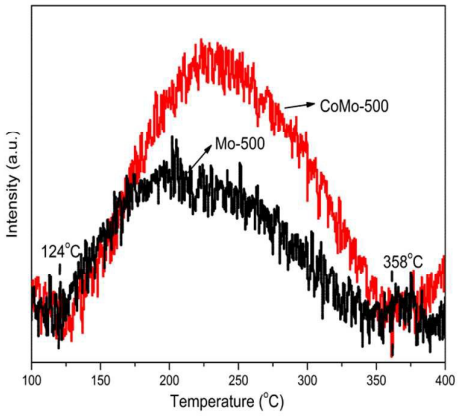


Fig. 4. $H_2$-TPD profiles of Mo-500 and CoMo-500 samples.

Fig. 4 gave the hydrogen temperature-programmed desorption ($H_2$-TPD) behavior on Mo-500 and CoMo-500 within the temperature range from 100 to 400 $^{o}$C. A typical hydrogen desorption peak was observed in the temperature range of 124-358$^{o}$C. It could be observed that, the amount of $H_2$ desorbed throughout the TPD appeared larger amount for the catalyst containing Co ions than the one without the Co, which predicted that the doping Co ions to $MoO_2$/CNTs improved the hydrogen adsorption capacity greatly. It could be stated that the a small amount Co ions addition is utilized as a catalyst structural modifier to induce more number of active sites available for $H_2$ chemisorbed and activate, resulting the excellent hydrogenation activity of Co doped $MoO_2$ catalyst. In addition, the temperature of the peak was close to the reaction temperature (200$^{o}$C), it is reasonable to speculate that hydrogen could be activated on the catalysts surface at the reaction temperature of 200$^{o}$C.

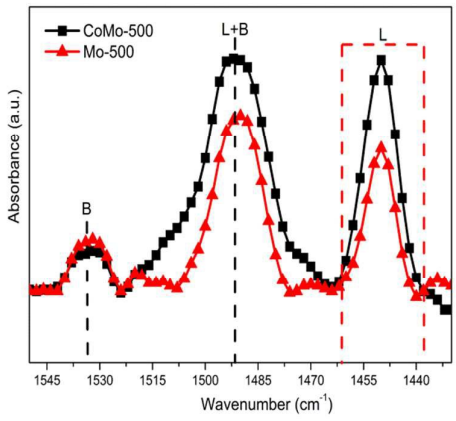


Fig. 5. Py-FTIR adsorption profiles of pristine Mo-500 and CoMo-500 samples.

In order to further understand the types and amount of the acidic sites of the catalyst, FT-IR spectrometry of adsorbed pyridine over Mo-500 and CoMo-500 were performed in Fig. 5. Both the catalysts possessed Brønsted acid sites (1536 $cm^{-1}$) and Lewis acid sites (1445 $cm^{-1}$), the absorbance at 1488 $cm^{-1}$ were assigned to pyridine on both Brønsted and Lewis acid sites (B + L).[32] Compared with Mo-500, a stronger relative intensity of Lewis acid sites existed on the CoMo-500 catalyst surface, which meaned that Co could promote the generation of Lewis acid sites. It had been reported that mixed oxides show much stronger acidic properties than single oxides.[29] The enriched acidic properties of mixed oxides were considered to be the result of an excess negative charge or positive charge induced by the formation of non-equivalent $M_1$-O-$M_2$ bonds, that is, it appeared that the doping of Co ions into the $MoO_2$ lattice (evidenced from XRD) results in the non-equivalent Co-O-Mo bonds and formation of oxygen vacancies in the vicinity of the dopant. As was well known, the oxygen vacancy was expected to behave as a Lewis acid site.[14] Thereby, the prepared CoMo-500 catalyst in the present work showed improved Lewis acidic nature compared to the Mo-500, which might be one of the key reasons to tailor the catalytic performance.

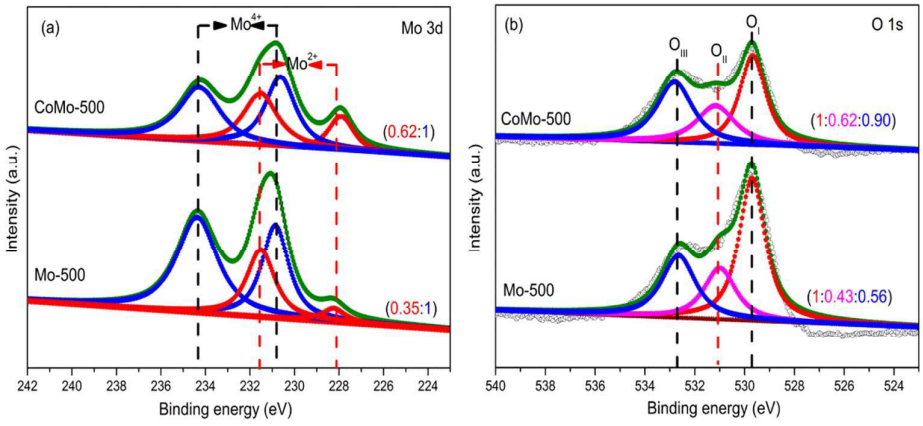

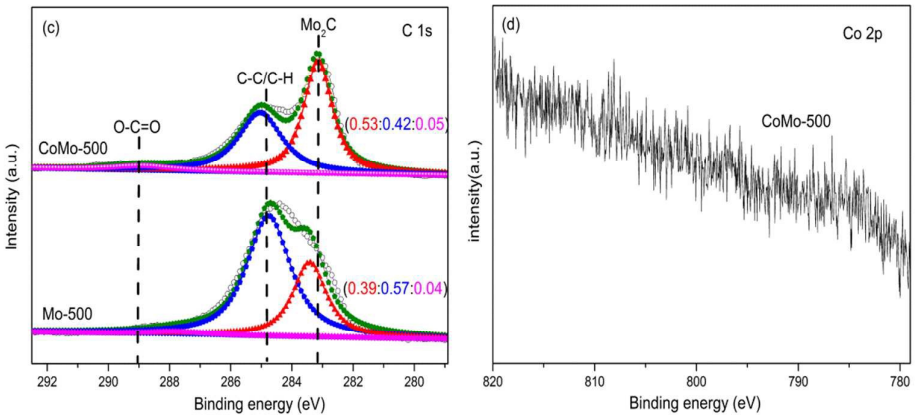


Fig. 6. XPS of Mo-500 and CoMo-500 samples (a) Mo 3d; (b) O 1s; (c) C 1s; and (d) Co 2p.

The characterization of chemical species located in the near-surface region of the catalysts was carried out by XPS. Fig. 6(a) depicted the Mo 3d core-level XPS of CoMo-500 and Mo-500 catalysts. The Mo $3d_{5/2}$ peak was centered at ~230.9eV, whereas the Mo $3d_{3/2}$ peak was found at ~234.2eV, with a spin energy separation of 3.3eV. This characteristic doublet of core-level Mo $3d_{5/2}$ and Mo $3d_{3/2}$ indicated the Mo (IV) oxidation state of $MoO_2$.[33, 34] In addition, the peaks at ~228.1 and ~231.6eV could be ascribed to Mo (II) $3d_{5/2}$ and $3d_{3/2}$ in $Mo_2C$, respectively.[35] After the incorporation of Co dopant, there was a small shift toward the lower binding energy side of the Mo 3d spectrum. A plausible explanation for this unusual observation could be the shift of electron density of the Co species toward the Mo, which indicated electronic modification of the Mo-O species with the incorporation of the Co into the $MoO_2$. The displacement of Mo 3d peaks also suggested the incorporation of Co ions into the $MoO_2$ lattice, which was consistent with the XRD, $H_2$-TPR and $H_2$-TPD. Additionally, the area ratio of the $Mo^{2+}$/ $Mo^{4+}$ on the surface of CoMo-500 (0.62) was quite higher than that of Mo-500 (0.35), indicating that the dopant Co ions could enhance the formation of $Mo^{2+}$ species. No peaks related to other molybdenum species were noted in the present investigation (i.e., $Mo^0$ at ~227.6eV and $Mo^{6+}$ at ~235.6eV).[36, 37]

Similar to that of the reported Co doped Ni-Mo-B catalyst, [36] the electronic states of oxygen in CoMo-500 were essentially modified with the doping of Co. As was can be seen from Fig. 6(b), O 1s XPS signals for both the catalysts could be fitted by three kinds of oxygen atoms, $O_I$ (BE = 529.8eV), $O_{II}$ (BE = 531.1eV), and $O_{III}$ (BE = 532.7eV). The $O_{III}$ component with a high BE of 532.7eV was assigned to the oxygen

chemisorbed loosely, such as $H_2O$ or $-CO_3^{2-}$ on the surface.[38] The medium-BE component $O_{II}$, centered at 531.1eV, was associated with $O^{2-}$ ions near the oxygen deficient within the matrix of $MoO_2$.[20, 39] The low-BE component $O_I$ at 529.8 eV was attributed to $O^{2-}$ ions of the $MoO_2$ crystal lattice. Among the $O_I$, $O_{II}$ and $O_{III}$ peaks, the $O_{II}$ peak was very important as it represents the existence of lattice defects (i.e., oxygen vacancies) in $MoO_2$. To evaluate the density of oxygen vacancies in the catalysts, the $O_{II}/O_{II}+O_I$ and $O_{II}$/Mo ratio ratios were used. The calculated values for CoMo-500 catalyst ($O_{II}/O_{II}+O_I$=0.38, $O_{II}$/Mo=0.089) were larger than Mo-500($O_{II}/O_{II}+O_I$=0.30, $O_{II}$/Mo=0.071), which meaned that the surface oxygen vacancies of CoMo-500 were more than that of Mo-500. It is a well-established fact in the literature[29] that the incorporation of smaller sized metal ions induces the shifting of neighboring O atoms towards dopants. The induced O distortions could enhance the lattice strain that would be relaxed by the formation of an O vacancy in the vicinity of the dopant. It was clear from the XRD studies that Co ions doped $MoO_2$ sample showed the increase of lattice distortion and reasonably large amount of oxygen vacancies than that of the pristine.

The higher solution C 1s spectrums of the CoMo-500 and Mo-500 catalysts were shown in Fig. 6(c). It can be deconvolved into three peaks corresponding to carbon atoms in different oxygen-containing functional groups. The strong C 1s peak at ~284.8eV was related to the nonoxygenated carbon in CNTs, while the weaker ones at ~289.1eV corresponds to carboxylate carbon (O-C=O).[37, 40] In the C1s XPS region, a peak at around 283.1 eV was detected for the catalysts, confirming the formation of $Mo_2C$ in these catalysts, resulting from the slight surface carbonization of $MoO_2$ in hydrogen.[41, 42] It is generally accepted that after $Mo_2C$ formation, there was a charge transfer from molybdenum to interstitial carbon atoms. The electron transfer results in the increase of the electron densities of these carbon atoms. It was observed that the area ratios of $C_{Mo_2C}/C_{C\text{-}C/C\text{-}H}$ of CoMo-500 (1.26) was much higher than that of Mo-500 (0.68), suggesting that addition of a second metal Co promoted the formation of $Mo_2C$ on the $MoO_2$ /CNTs surface. In agreement with the observations by Li and co-workers, [43] we posited that during the $H_2$ reduction, the second Co metal promotes formation of CHx species from reactive carbon atoms or groups on CNTs and hydrogen, which further carburized oxide precursors.

The Co 2p XPS of the CoMo-500 sample were presented in Fig. 6(d). No signals associated with surface Co species, such as $Co^{3+}$, $Co^{2+}$ and $Co^0$ ions, were noted in the

investigated region. This notable scrutiny can be explained due to doping of Co ions into the $MoO_2$ lattice, which was consistent with the result of XRD. ICP-AES analysis results also certified the existence of Co ionic in the Co-doped catalyst.

**Catalytic Activity**

Long-chain fatty acids represented a significant fraction (about 30~50%) in the bio-oil obtained from thermochemical conversion of algal biomass.[4] Thus, palmitic acid was used as the probe molecule in this study. The HDO of palmitic acid over Mo-500 and CoMo-500 catalysts were investigated and the results were shown in table 2. As was expected, the doping of Co significantly improved the catalytic performances of CoMo-500. As was shown in Table 2, the palmitic acid conversion over Mo-500 catalyst was only 51.5% and the hexadecane selectivity was 7.8% at 200 $^{o}$C. However, in our investigation, the conversion of palmitic acid over CoMo-500 was high up to 100% with a selectivity of 91.1% hexadecane at 200 $^{o}$C, which was much higher than that of Mo-500. When performing the reaction at a lower temperature (180 $^{o}$C), large amounts of hexadecanol could be observed. As our previous report, the dehydration of the intermediate alcohol was the rate-determining step in the overall reaction.[17] The main reaction pathway for catalytic HDO of palmitic acid to hexadecane was presented in Table 2.

Considering the results of various characterization techniques, we knowed that Co had doped into the lattice of $MoO_2$ and the interaction between metal species modified the electrical properties of the catalytic active sites, formation of defects (both structure and electronic defects) and new active sites, thus affecting the adsorption state of the substrate and hydrogenation/ deoxygenation activity. As could be noted from Table 3, compared to Mo-500, CoMo-500 catalyst contained a larger amount of $Mo_2C$ particles, Lewis acid sites and oxygen vacancies. According to the literature reports, [14] oxygen vacancies could weaken C-O bond upon adsorption of the acid/alcohol molecule on the active site, and such bond weakening would allow the dehydration of the acid or intermediate alcohol species easily to occur. Mortensen and co-workers [44] concluded that the best performing hydrogenation catalyst was therefore the catalyst with the strongest tendency to form Lewis acid sites in the oxide structure. Thus, the Lewis acid was responsible for the activation of both the oxy compound and hydrogen on the catalyst surface, which was beneficial for HDO reaction.[45] Additionally, $Mo_2C$ was well known as the active sites for HDO of oxygenates and

selective toward hydrocarbon productions.[41] Thus, the high content of $Mo_2C$ particles on the CoMo-500 surface was another reason for the enhanced activity due to its excellent HDO activity. Hence, we proposed that the high content of $Mo_2C$ particles, Lewis acid sites and oxygen vacancies might be the reasons for the high HDO activity of CoMo-500 catalysts.

**Table 2** Conversion of palmitic acid and selectivity of products over Mo-500 and CoMo-500 catalysts

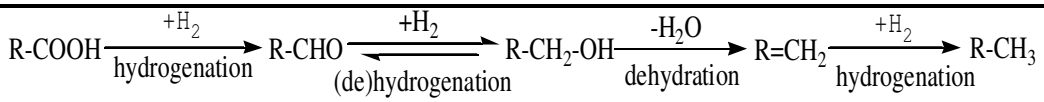


| Catalyst | Temperature (°C) | Conversion (%) | Component distribution (%) | | | |
|---|---|---|---|---|---|---|
| | | | Pentadecane | Hexadecane | Hexadecanol | palmitic acid |
| Mo-500 | 230 | 100 | 9.6 | 88.2 | 0 | 0 |
| Mo-500 | 200 | 51.5 | 2.0 | 7.8 | 40.9 | 48.5 |
| Mo-500 | 180 | 20.3 | ~ | 1.3 | 18.7 | 79.7 |
| CoMo-500 | 200 | 100 | 7.9 | 91.1 | 0 | 0 |
| CoMo-500 | 180 | 100 | 3.8 | 54.8 | 41.4 | 0 |
| CoMo-520 | 180 | 100 | 5.2 | 89.3 | 4.9 | 0 |
| CoMo-550 | 180 | 100 | 4.3 | 40.0 | 55.4 | 0 |
| Co-500 | 200 | 40.6 | 36.4 | 1.1 | 2.6 | 59.4 |
| Co-500 | 180 | 17.6 | 13.4 | 0 | 1.3 | 82.4 |
| blank | 200 | 10.3 | 3.4 | 2.0 | 0 | 89.7 |

Reaction conditions: palmitic acid (0.5 g), decane (50 mL), catalysts (0.1 g), $H_2$ (4MP), reaction time (4 h), and stirring at 300 rpm.

In order to further confirm the positive impact of surface $Mo_2C$ particles, Lewis acid sites and oxygen vacancies on catalytic activity, Co doped catalyst prepared by the incipient wetness impregnation method were reduced at 500, 520 and 550°C respectively. As was shown in Fig. 7(a) and (c), the relative content of $Mo_2C$ particles on the catalyst surface was increased with the increase of reduction temperature. Although higher reduction temperatures would be beneficial for the formation of $Mo_2C$ particles, it also led to the decrease of Lewis acid sites and oxygen vacancies.

In agreement with the observations by Ledoux and co-workers, [46] as the reduction temperature increased the degree of reduction increased, the $MoO_{2-x}$ structure underwent a shared-plane reconstruction, where in created oxygen vacancies were filled with carbon to create $Mo_2C$ particles. As was shown in Table 2, the conversion of palmitic acid and the selectivity of hexadecane were strongly dependent on the reduction temperature of the Co doped catalyst. The activity results showed that the catalyst precursors reduced at 520 $^oC$ had the highest catalytic activity, the conversion of palmitic acid was high up to 100 % with a selectivity of hexadecane as high as 89.3% at 180$^oC$. The catalytic activity of CoMo-550 was significantly higher than that of the Mo-500, even though they had similar amount of Lewis acid sites and oxygen vacancies. This suggested that the number of $Mo_2C$ particles impacted on the catalytic activity significantly. According to the Py-FTIR (Fig. 8) and XPS results, CoMo-520 had less Lewis acid sites and oxygen vacancies, more $Mo_2C$ particles than CoMo-500, but it presented a much higher HDO activity, indicating that the amount of oxygen vacancies and Lewis acid sites were not the dominant factors for the HDO activity and the amount of $Mo_2C$ should be the most important factor to improve catalytic activity in the present reaction. The fundamental reason might be due to the intrinsic high HDO activity of $Mo_2C$ nanoparticles. However, compared to CoMo-520, CoMo-550 did not show the highest activity although it had the maximum $Mo_2C$ particles. This means that the number of oxygen vacancies and Lewis acid sites also had a positive impact on the activity. In addition, CoMo-500 gave rise to a slightly higher hexadecane selectivity and a lower hexadecanol selectivity comparative to that on CoMo-550, further confirming the positive impact of oxygen vacancies and Lewis acid sites for catalytic dehydration of intermediate alcohol. Based on the experimental data presented above, we could see that the sequence of catalytic activity neither consistent with the amount of Lewis acid sites and oxygen vacancies nor the content of $Mo_2C$ particles. It could be concluded that the amount of Lewis acid sites, oxygen vacancies and $Mo_2C$ all play a crucial role in the HDO activity, and there was an optimal ratio between them. These active centers worked cooperatively, resulting in high activity for producing hexadecane.

On the basis of the above discussion and the literature results, the excellent HDO activity of Co doped catalysts could be explained by the following facts. The Co doped $MoO_2$ catalyst surface existed large amount of active centers, such as $Mo_2C$ particles, Lewis acid sites and oxygen vacancies and there existed a strong synergetic

effect between them, which guaranteed the HDO reaction went on smoothly. The HDO of palmitic acid to hexadecane could be uniquely catalyzed over different active centers on $MoO_2$ surface via two parallel pathways: one via hexadecane formation on $Mo_2C$ active centers, the second via a synergistic action by $Mo_2C$ and oxygen vacancies through adsorbing the carboxylic groups at the oxygen vacancies to form carboxylates and subsequently hydrogenated to hexadecane on $Mo_2C$ nanoparticles (as was shown in Scheme 2).

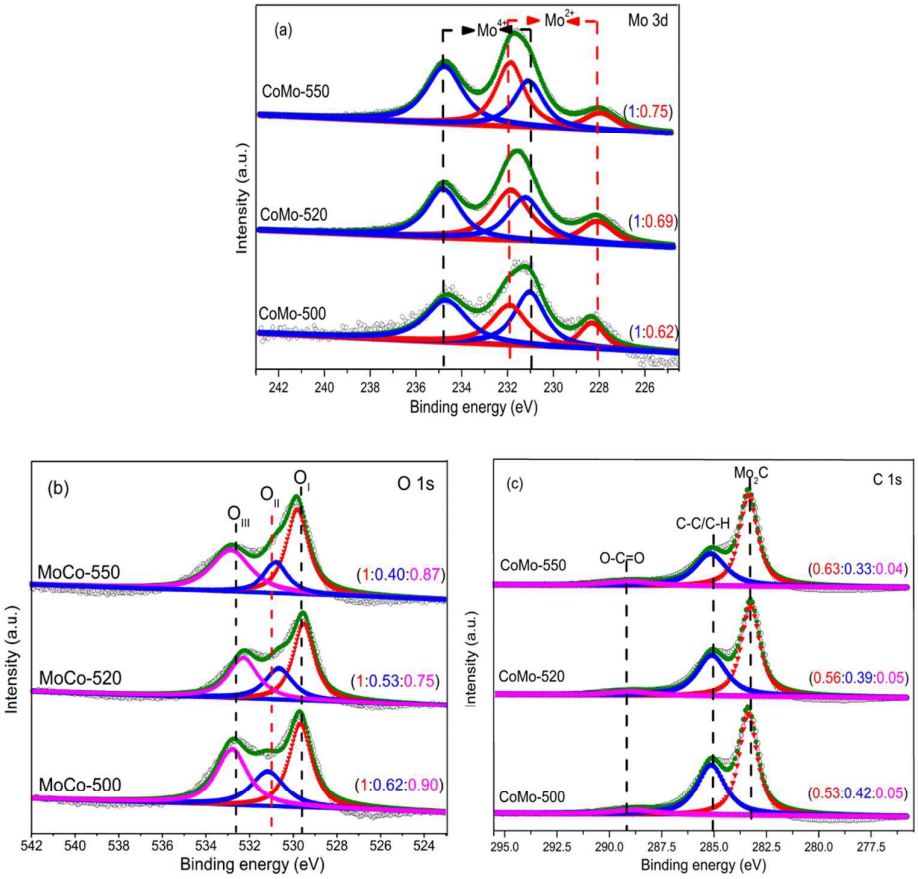


Fig. 7. XPS of CoMo-500, CoMo-520 and CoMo-550 samples. (a) Mo 3d; (b) O 1s; and (c) C 1s

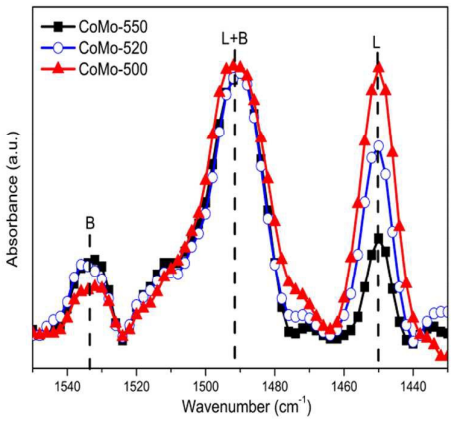


Fig. 8. Py-FTIR adsorption profiles of CoMo-500, CoMo-520 and CoMo-550 samples.

**Table 3** Correlation between amount of Lewis acid sites, area ratios of $C_{Mo2C}/C_{C\text{-}C/C\text{-}H}$, area ratios of $O_{II}/O_{II}+O_I$ and catalytic activity results of Co-doped samples reduced at 500, 520, and 550°C respectively.

| Catalyst | [a]$C_{Mo2C}/C_{C\text{-}C/C\text{-}H}$ | [b]$O_{II}$/Mo | [c]$O_{II}/O_{II}+O_I$ | [d]Lewis acid sites (μmol $g^{-1}$) | [e]Conversion (%) | [f]Hexadecane selectivity(%) |
|---|---|---|---|---|---|---|
| Mo-500 | 0.68 | 0.071 | 0.30 | 14.5 | 20.3 | 1.3 |
| CoMo-500 | 1.26 | 0.089 | 0.38 | 22.3 | 100 | 54.8 |
| CoMo-520 | 1.44 | 0.081 | 0.35 | 15.6 | 100 | 89.3 |
| CoMo-550 | 1.91 | 0.065 | 0.29 | 10.7 | 100 | 40.0 |

[a, b,c] From XPS analysis. [d] From FTIR analysis of adsorbed pyridine. [e,f] From table 2.

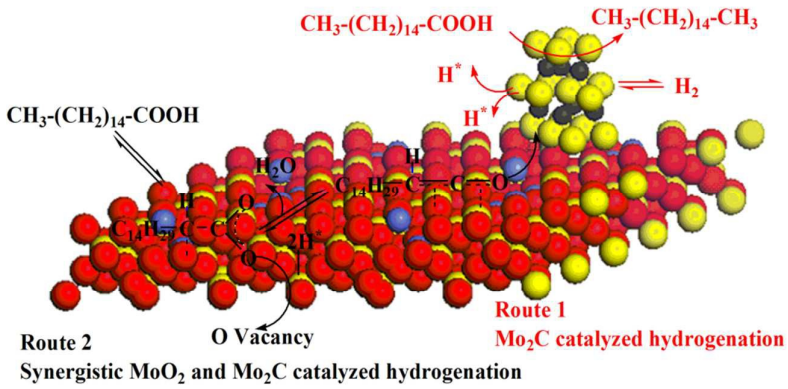


Scheme 2. Scheme for palmitic acid HDO on the surface of CoMo-500 catalyst.

## Catalyst stability Studies

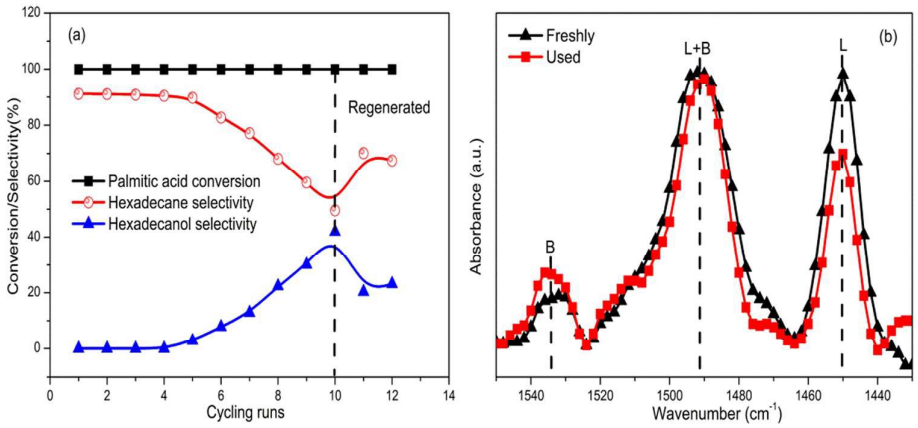


Fig.9. (a) Cycling runs tests (reaction temperature at 200°C) of CoMo-500 catalyst and (b) Py-FTIR adsorption profiles of freshly prepared and used ten times CoMo-500 samples.

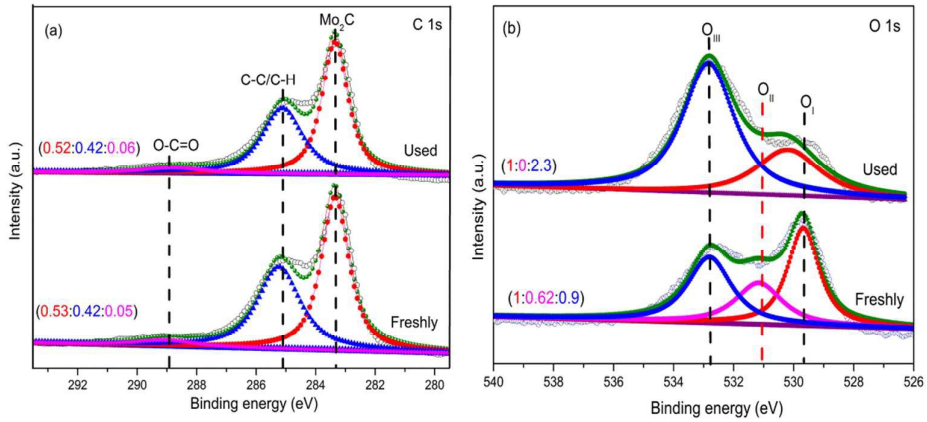


Fig.10. XPS of freshly prepared and used ten times CoMo-500 samples. (a) C 1s and (b) O 1s.

We also investigated the reusability of CoMo-500 catalyst to understand its stability for the HDO of palmitic acids (Fig. 9a). The catalytic experimental conditions were conducted with the same as described in Table 2. After each cycle, the catalyst was separated from the reaction mixture by centrifugation and dried in an oven at 105°C for 10 min before the next catalytic run. It was interesting to note that the catalyst could be recycled up to a ten run without considerable variation in the conversion of palmitic acid. The selectivity to hexadecane was gradually decreased from 91.1 to 49.6 % with the increased of corresponding hexadecanol after the repeated use of catalyst for up to ten catalytic runs. Generation study confirmed that catalytic activity and selectivity could be partially recovered when calcining the catalyst use of pure $H_2$ at 500°C for 1 h.

To gain a better understanding of the significant variation in the selectivity of products, the spent catalysts after the tenth cycle were characterized using XRD, Py-FTIR, FT-IR, BET and XPS. The obtained results were compared with that of the fresh catalyst. It could be noticed from XRD test that the position and the intensity of diffraction peaks of CoMo-500 were nearly the same to the fresh catalyst, the framework of $MoO_2$ structure remained intact without any signs of collapse (Supporting Information, Fig. S1). The Mo 3d XPS spectra of the spent catalyst were nearly superimposable to the fresh catalyst, no obvious change of the Mo oxidation state after the tenth cycle (Supporting Information, Fig. S2). Moreover, the relative intensity of XPS peak of $C_{Mo2C}$ in the used CoMo-500 catalyst showed almost no decrease, indicating that no significant change of the amount of $Mo_2C$ active sites (Fig. 10a). These results all clearly indicated the stability of CoMo-500 catalyst. As was shown in XPS spectra of O 1s (Fig. 10b), the relative intensity of the XPS peak of $O_{II}$ (related to oxygen vacancies) in the used CoMo-500 catalyst vanished and the $O_{III}$ peak increased, indicating that the adsorbed of oxygen species on oxygen vacancies during the runs. This was also been evidenced by the FT-IR (Supporting Information, Fig. S3). The relative intensity of FT-IR peaks corresponding to oxygen species of the used catalyst was stronger than the fresh ones, indicating that the adsorbed of oxygen species on catalyst surface. Moreover, as was shown in Fig. 9(b), the total amount of Lewis acidic sites presented on the surface of spent catalyst also decreased compared to the fresh catalyst. The decrease of Lewis acidic sites observed after the tenth cycle could be explained by a decrease in the number of oxygen vacancies occupied by parent reactant or intermediates as evidenced by the XPS. As the previous discussed, the oxygen vacancy sites were responsible for weaken of the C-O bond of hexadecanol on the active site, which guaranteed the dehydration reaction went on smoothly. Therefore, the decrease of oxygen vacancy sites was one of the key reasons for decrease of hexadecane selectivity and higher hexadecanol selectivity. The $N_2$ adsorption-desorption isotherms and pore size distribution curves of the fresh and spent catalysts were shown in Fig. S4. It was found that the spent catalyst exhibits decreased BET surface area (~84 $m^2/g$) compared to fresh catalyst (~104 $m^2/g$). The pore volume was found to decrease from 0.572 to 0.428$cm^3/g$, which might be due to the structure destruction of the support CNTs. Therefore, it could be concluded that the decreased of surface oxygen vacancies and the BET surface area were both responsible for the decrease selectivity of hexadecane during the successive reactions.

On the whole, the CoMo-500 catalyst was quite stable and recyclable in the HDO of palmitic acid under ambient reaction conditions.

## Conclusions

In summary, we had demonstrated that Co has a significant effect on the activity and selectivity of $MoO_2$-based catalyst for the HDO of palmitic acid. The promoting role of dopant Co on the physicochemical properties of $MoO_2$-based catalyst were also been investigated by means of various characterization techniques. XRD results suggested formation of nanocrystalline $MoO_2$ solid solutions due to the incorporation of Co ion into the $MoO_2$ lattice. Py-FTIR showed that larger amounts of Lewis acidic sites were found for Co doped sample as compared to pristine $MoO_2$, and the TPR results confirmed facile reduction of the doped $MoO_2$. XPS measurements suggested the formation of more $Mo_2C$ particles and oxygen vacancies on the surface of the doped catalysts, and the $H_2$-TPD results confirmed enhanced hydrogen adsorption capacity of the Co doped catalyst. The increased presence of $Mo_2C$ particles, Lewis acidic sites and oxygen vacancies were found to be the decisive factors for better catalytic activity of the Co-doped catalyst and there existed a synergetic effect between them. These active centers worked cooperatively, resulting in high activity for producing hexadecane. The catalyst recycling test suggested that the Co-doped catalyst was quite stable and recyclable in the HDO of palmitic acid. The selectivity of hexadecane decreased with repeated use due to the reduced concentration of oxygen vacancies accompanied with decreased BET surface area. This new kind of amorphous catalyst with low cost, simple preparation, high thermal stability and high HDO activity would be a potential candidate for the HDO process of algal bio-oil.

## Acknowledgments

This work was supported by the National Science Foundation of China (No. 21376140and No.21176142), Program for Chang jiang Scholars and Innovative Research Team in University（IRT13026）and Program for New Century Excellent Talents in University (No. NCET-12-0308).

## References

1 J. G. Na, B. E. Yi, J. K. Han, Y. K. Oh, J. H. Park, T. S. Jung, S. S. Han, H. C. Yoon, J. N. Kim, H. Lee and C. H. Ko, Energy, 2012, 47, 25-30.

2 R. W. Gosselink, D. R. Stellwagen and J. H. Bitter, Angew. Chem., 2013, 125, 5193-5196.
3 B. X. Peng, X. G. Yuan, C. Zhao and J. A. Lercher, J. Am. Chem. Soc., 2012, 134, 9400-9405.
4 S. P. Zou,Y .L. Wu, M. D. Yang, C. Li and J. M. Tong, Energ. Environ. Sci., 2010, 3, 1073-1078.
5 P. G. Duan and P. E. Savage, Appl. Catal. B: Environ., 2011, 104, 136-143.
6 Y. Zeng, B. H. Zhao, L. F. Zhu, D. M. Tong and C. W. Hu, RSC Adv., 2013, 3,10806-10816.
7 V. A. Yakovlev, S. A. Khromova, O. V. Sherstyuk, V. O. Dundich, D. Y. Ermakov, V. M. Novopashina, M. Y. Lebedev, O. Bulavchenko and V. N. Parmon, Catal. Today, 2009, 144, 362-366.
8 T. Prasomsri, T. Nimmanwudipong, Y. Román-Leshkov, Energ. Environ. Sci., 2013, 6, 1732-1738.
9 J. X. Han, H. Sun, Y. Q. Ding, H. Lou and X. M. Zheng, Green Chem., 2010, 1, 463-467.
10 S. A. W. Hollak, J. H. Bitter, J. van Haveren, K. P. de Jong and D. S. van Es, RSC Adv., 2012, 2, 9387-9391.
11 J. X. Han, J. Z. Duan, P. Chen, H. Lou and X. M. Zheng, Adv. Synth. Catal., 2011, 353, 2577-2583.
12 B. X. Peng, Y. Yao, C. Zhao and J. A. Lercher, Angew. Chem. Int. Ed., 2012, 51, 2072-2075.
13 E. S. Jimenez and M. Crocker, J. Chem. Technol. Biotechnol., 2012, 87, 1041-1050.
14 T. Prasomsr, M. Shetty, K. Murugappan, Y. Román-Leshkov, Energ. Environ. Sci., 2014, 7, 2660-2669.
15 D. H. Mei, A. M. Karim and Y. Wang, J. Phys. Chem. C, 2011, 115, 8155-8164.
16 L. Boda, G. Onyestyák, H. Solt, F. Lónyi, J. Valyon and A. Thernesz, Appl. Catal. A: Gen., 2010, 374,158-169.
17 R. R. Ding, Y. L. Wu, Y. Chen, J. M. Liang, J. Liu and M. D. Yang, Chem. Eng. Sci., Inpress, Doi: 10.1016/j.ces.2014.10.024.
18 X. R. Li, C. Zhang, H. Y. Cheng, L. M. He, W. W. Lin, Y. C. Yu and F. Y. Zhao, J. Mol. Catal. A: Chem., 2014, 395, 1-6.
19 H. Y. Cheng, W. W. Lin, X. R. Li, C. Zhang and F.Y. Zhao, Catal., 2014, 4, 276-288.
20 X. R. Li, C. Zhang, H. Y. Cheng, W. W. Lin, P. J. Chang, B. Zhang, Q. F. Wu, Y. C. Yu and F. Y. Zhao, ChemCatChem, 2015, 7, 1322-1328.
21 B. Mallesham, P. Sudarsanam and B. M. Reddy, Ind. Eng. Chem. Res., 2014, 53, 18775 -18785.
22 W. Sun, Y. Song, X. Q. Gong, L.M. Cao, and J. Yang, Chem. Sci., 2015, 6, 4993-4999.
23 W. Y. Wang, Y. Q. Yang, H. Luo, T. Hu, W. Y. Liu, Catal. Commun., 2011, 12, 436-440.
24 X. S. Niu, H. H. Li and G. G. Liu, Mol. Catal. A: Chem., 2005, 232, 89-93.
25 K. Soongprasit, D. Aht-Ong, V. Sricharoenchaikul and D. Atong, Curr. Appl. Phys., 2012, 12, S80-S88.

26 L. Kumari, Y. R. Ma, C. C. Tsai, Y. W. Lin, S. Y. Wu, K. W. Cheng and Y. Liou, Nanotechnology, 2007,18,1-7.

27 Y. L. Liu, H. Zhang, P. Ouyang and Z. C. Li, Electrochim. Acta., 2013, 102, 429-435.

28 J. X. Han, J. Z. Duan, P. Chen, H. Lou, X. M. Zheng and H. P. Hong, Green Chem., 2011,13, 2561-2568.

29 B. Mallesham, P. Sudarsanam, G. Raju and B. M. Reddy, Green Chem., 2013, 15, 478-489.

30 M. Dieterle and G. Mestl, Chem. Chem. Phys., 2002, 4, 822-826.

31 Y. M. Sun, X. L. Hu, J. C. Yu, Q. Li, W. Luo, L. X. Yuan, W. X. Zhang and Y. H. Huang, Energy Environ. Sci., 2011, 4, 2870-2877.

32 A. S. Poyraz, C. H. Kuo, E. Kim, Y. T. Meng, M. S. Seraji and S. L. Suib, Chem. Mater. 2014, 26, 2803-2813

33 Z. Song, T. H. Cai, Z. P. Chang, G. Liu, J. A. Rodriguez and J. Hrbek, J. Am. Chem. Soc., 2003, 125, 8059-8066.

34 T. Schroeder, J. Zegenhagen, N. Magg, B. Immaraporn and H. J. Freund, Surf. Sci., 2004, 552, 85-97.

35 J. A. Schaidle, A. C. Lausche and L. T. Thompson, J. Catal., 2010, 272, 235-245.

36 W. Y. Wang, Y. Q. Yang, H. Luo and W. Y. Liu, Reac. Kinet. Mech. Cat., 2010, 101, 105-115.

37 Y. M. Sun, X. L. Hu, W. Luo and Y. H. Huang, Nano., 2011, 5, 7100-7107.

38 H. Xia, D. D. Zhu, Z. T. Luo, Y. Yu, X. Q. Shi, G. L. Yuan and J. P. Xie, Sci. Rep., 2013, 3, 2978-2985.

39 J. H. Li, H. J. Fu, L. X. Fu and J. M. Hao, Environ. Sci. Technol., 2006, 40, 6455-6459.

40 L. Detomaso, R. Gristina, G. S. Senesi, R. d'Agostino and P. Favia, Biomaterials, 2005, 26, 3831-3841.

41 J. X. Han, J. Z. Duan, P. Chen, H. Lou, X. M. Zheng and H.P. Hong, ChemSusChem, 2012, 5, 72-733.

42 J. Li, L. T. Liu, Y. Liu, M. Z. Li, Y. H. Zhu, H. C. Liu, Y. Kou, J. Z. Zhang, Y. Han and D. Ma, Energy Environ. Sci., 2014, 7, 393-398.

43 C. H. Liang, W. P. Ma, Z. C. Feng and C. Li, Carbon, 2003, 41, 1833-1839.

44 P. M. Mortensen, J. D. Grunwaldt, P. A. Jensen and A. D. Jensen, ACS Catal., 2013, 3, 1774 -1785.

45 J. Guan, G. M. Peng, Q. Cao and X. D. Mu, J. Phys. Chem. C, 2014, 118, 25555-25566.

46 P. Delporte, F. Meunier, C. Pham-Huu, P. Vennegues, M. J. Ledoux and J. Guille, Catal. Today, 1995, 23, 251-267.

# Catalytic Hydrodeoxygenation of Palmitic Acid over Bifunctional Co-doped $MoO_2$/CNTs Catalyst: an Insight into the Promoting Effect of Cobalt

Ranran Ding[a], Yulong Wu[a,b]*, Yu Chen[a], Hao Chen[c], Jianlong Wang[a], Yanchun Shi[a], Mingde Yang[a]

[a]Institute of Nuclear and New Energy Technology, Tsinghua University, Beijing 100084, PR China
[b]Beijing Engineering Research Center for Biofuels, Beijing 100084, PR China
[c]School of chemical engineering and technology, Xi'an Jiaotong University, Xi'an 710049, PR China

E-mail address: wylong@tsinghua.edu.cn

Tel.: (+86) 10-89796163; Fax: (+86) 10-62784831

In this work, hydrodeoxygenation (HDO) of palmitic acid into $C_{16}$ hydrocarbons was successfully achieved over Co doped $MoO_2$/CNTs catalysts at a much lower temperature (180$^{o}$C). The promoting role of dopant Co on the physicochemical properties of $MoO_2$/CNTs were been investigated by means of various characterization techniques. It was found that the Co could promote the formation of Lewis acidic sites, oxygen vacancies and $Mo_2C$ particles, which are all the decisive factors for better catalytic activity of the catalyst and these active centers work cooperatively. The mechanistic insights from this work confirmed the bifunctional role of Co-doped $MoO_2$/CNTs catalysts for HDO of palmitic acid, which is catalyzed either solely by $Mo_2C$ or synergistically by $Mo_2C$ and the $MoO_2$.

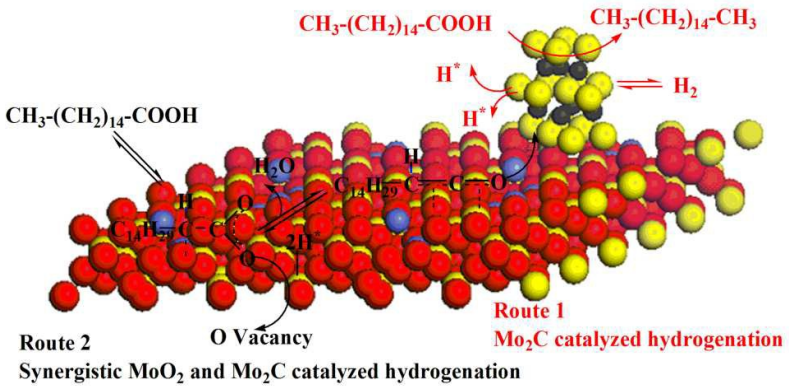


Scheme for HDO of palmitic acid on the surface of Co-doped $MoO_2$/CNTs catalyst